Microfluidic Feed Forward Loop Pulse Generator for Molecular Communication

Yansha Deng, *Member, IEEE,* Massimiliano Pierobon, *Member, IEEE,* Arumugam Nallanathan, *Fellow, IEEE.*

***Abstract*—The design of communication systems capable of processing and exchanging information through molecules and chemical processes is a rapidly growing interdisciplinary field, which holds the promise to revolutionize how we realize computing and communication devices. While molecular communication (MC) theory has had major developments in recent years, more practical aspects in the design and prototyping of components capable of MC functionalities remain less explored. In this paper, motivated by a bulk of MC literature on information transmission via molecular pulse modulation, the design of a pulse generator is proposed as an MC component able to output a predefined pulse-shaped molecular concentration upon a triggering input. The chemical processes at the basis of this pulse generator are inspired by how cells generate pulse-shaped molecular signals in biology. At the same time, the slow-speed, unreliability, and non-scalability of these processes in cells are overcome with a microfluidic-based implementation based on standard reproducible components with well-defined design parameters. Mathematical models are presented to demonstrate the analytical tractability of each component, and are validated against a numerical finite element simulation. Finally, the complete pulse generator design is implemented and simulated in a standard engineering software framework, where the predefined nature of the output pulse shape is demonstrated together with its dependence on practical design parameters.**

I. Introduction

The possibility of harnessing information processing and communication functionalities from chemical and physical processes at the level of molecules has been at the basis of a great bulk of research in recent years on Molecular Communication (MC) [1]–[4]. Despite substantial developments in the theoretical study of MC, the design and prototyping of components capable of MC functionalities has been a much less developed area, partly because of the highly interdisciplinary technical knowledge and tools required to practically engineer these systems.

In this paper, motivated by a bulk of MC literature on information transmission via molecular pulse modulation [5,6], where a single or multiple types of molecules are emitted according to pulse-shaped signals to represent symbols in a digital message, we propose the design of a pulse generator component for MC systems. With reference to pulse generation in electrical systems, the proposed design generates molecular concentration pulses with a predefined shape according to an input trigger signal exclusively by means of chemical and physical processes in the molecular domain. The shape of the pulse is predictable a priori and reproducible as a function of component design parameters, thus potentially providing a platform for the definition of a standard pulse shape for MC [7].

The chemical processes at the basis of the proposed pulse generator are inspired by how cells process molecular signals in biology [8]. In particular, studies have revealed how a specific pattern of chained biochemical reactions underlying the regulation of cells' DNA expression, *i.e.*, gene regulatory network, results in the capability of generating pulse-shaped molecular concentration signals [9]. While the utilization of biological cells for molecular communication currently faces challenges such as slow speed, unreliability, and non-scalability [10], we propose a microfluidic-based implementation of the aforementioned chemical pattern based on standard reproducible components with well-defined design parameters.

The design of the proposed pulse generator is supported in this paper by both analytical and numerical simulation results. In particular, we present an analytical framework of the microfluidic components of the pulse generator based on convection-diffusion and the convection-diffusion-reaction equations in microfluidic systems, where input-output relations of each components, based on a 1D approximation of the microfluidic channels, are expressed as a function of design parameters, such as the length of each microfluidic channel, and the rates of the chemical reactions. These analytical results are validated against simulations performed through the COMSOL Multiphysics finite element solver. Finally, the complete pulse generator design is implemented and simulated in the COMSOL Multiphysics environment, where the dependence of different predefined output pulse shapes on the aforementioned design parameters is numerically evaluated.

The rest of the paper is organized as follows. In Sec. II we present the overall pulse generator design and motivate it in light of our abstraction of gene regulatory networks through a chemical reaction network in a microfluidic system. In Sec. **??** we detail and numerically evaluate the analytical models of the pulse generator components, while in Sec. **??** we present the implementation and numerical simulation results of the overall design in COMSOL Multiphysics. Finally, in Sec. V we conclude the paper.

This work was supported by the US National Science Foundation (NSF) through grant MCB-1449014.

Y. Deng and A. Nallanathan are with Department of Informatics, King's College London, London, WC2R 2LS, UK (email:{yansha.deng, arumugam.nallanathan}@kcl.ac.uk).

M. Pierobon is with the Molecular and Biochemical Telecommunications (MBiTe) Lab, Department of Computer Science and Engineering, University of Nebraska-Lincoln, Lincoln, NE 68588, USA (email: pierobon@cse.unl.edu).

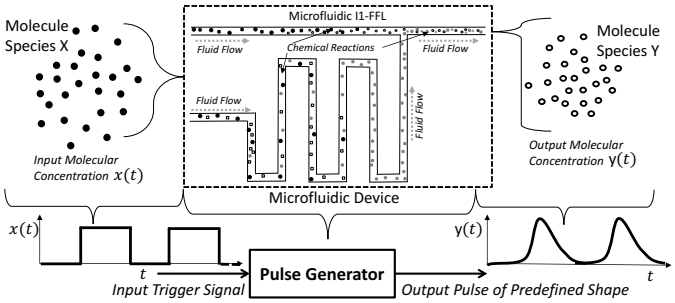

Fig. 1. Overall scheme of the proposed pulse generator for MC.

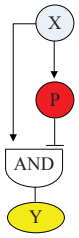

Fig. 2. The I1-FFL network motif.

II. A Pulse Generator for Molecular Communication

The overall scheme of the proposed pulse generator for MC is shown in Fig. 1, where an input molecular signal composed of molecules of species X in a fluid and concentration $x(t)$ as a function of the time t is the input trigger of a microfluidic device that upon a variation in the concentration $x(t)$ produces as output another molecular signal composed of molecules of species Y and concentration $y(t)$ that varies as a function of the time t by following a predefined pulse shape. This pulse shape is dependent on the values of parameters in the microfluidic device implementation. As the fluid containing the molecules of species X flows through the microfluidic device channels, a series of chemical reactions with other molecules generate the molecules of species Y according to the aforementioned desired pulse signal. This microfluidic device design, detailed in Sec. **??**, is directly inspired by the incoherent type 1 feed forward loop motif in gene regulatory networks [10], described next.

A. The FFL Motifs in Gene Regulatory Networks

Gene regulatory networks are sets of interconnected biochemical processes in a biological cell [11], where DNA genes are linked together by activation and repression mechanisms of certain biological macromolecules that regulate their expression into proteins. Each DNA gene contains coding sequences, which are chemical information for building proteins, and regulatory sequences, which are sites the proteins (transcription factor) can bind and control the rate of the gene expression, either by increasing (activation) or decreasing (repression) the rate of protein synthesis. In gene regulatory networks, genes are interconnected such as the proteins produced by one or more genes regulate the expression of one or more genes, thus resulting in complex protein expression dynamics.

Gene regulatory networks can be abstracted with nodes representing the genes, interconnected by directed edges that correspond to the control of a gene (edge destination) expression by a transcription factor encoded by another gene (edge source). Network motifs are patterns of nodes and directed edges that occur more frequently in natural gene transcription networks than randomized networks [8]. The FFL is a family of network motifs among all three-node patterns frequently observed in nature [8,9]. In the structure of FFL, the transcription factor protein X regulates the genes expressing other two proteins, namely, P and Y, where P is also a transcription factor that regulates the gene expressing protein Y. Depending on the types of these regulations, either activation or repression, there are 8 different of FFLs [10].

Among other FFLs found in nature, the Incoherent type 1 FFL (I1-FFL) results in a pulse-like dynamics of its output Y [9]. As shown in Fig. 19, an input gene expresses the protein X, which is a transcription factor for the genes expressing Y and P. In presence of X, the expression of the genes encoding protein Y and protein P are activated, resulting in the build up of the concentrations of protein Y and protein P, respectively. On its turn, the protein P is another transcription factor that works as a repressor for the gene encoding protein Y. The AND input to the gene that encodes Y corresponds to a situation where this gene is activated when the transcription factor X binds to the regulatory sequence, but it is inactivated whenever transcription factor P binds to the same sequence independently from the presence of X. In such a way, protein X initializes the rapid expression of the gene encoding protein Y first, and after a delay, enough P accumulates and represses the production of protein Y, whose concentration will continuously decrease because of natural degradation. This generates a pulse shape for the concentration of protein Y as a function of the time.

One example of I1-FFL is the galactose system of *E. coli*, where the galactose utilization operon (a cluster of genes sharing the same regulatory sequences and expressed together) galETK is regulated in an I1-FFL by the activator CRP (X), and the repressor $GalS$ (P) [12]. Results shown that in nature we can observe a pulse-like expression of the galETK genes, which is initiated by a step variation of active CRP mediated by the molecular species $cAMP$ (S_x).

In this paper, we take inspiration from the I1-FFL to design a pulse generator in the molecular domain. Although the discipline of synthetic biology is opening the road to the programming of functionalities in the biochemical environment through genetic engineering of biological cells [13], there are a number of factors that encouraged an alternative technology for the design of a pulse generator in this paper, such as the small number of molecules involved for each cell together with difficulties in coordinating multiple cells, the added complexity of cellular behavior, including cell growth, evolution, and biological noise, and the slow response time of genetic regulatory networks such as the I1-FFL, whose output pulse shape is usually realized in nature in the order of cell generation time (hours) as indicated in [12, Fig. 4].

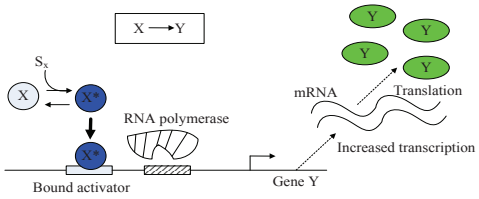

Fig. 3. Promoter.

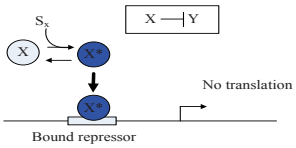

Fig. 4. Repressor.

B. FFL Biological Circuits

The recent advances in synthetic biology toward the engineering of DNA-based circuits has provided a promising pathway for the realization of biological nanoscale devices via programming man-designed functions inside biological cell [10]. More specifically, a synthetic biological circuit, also called biological circuit, enables the logical function programming via controlling the protein production, for the purpose of achieving cell-to-cell interactions.

1) Gene Regulation: To better illustrate the FFL biological circuits, the underlying biological theory behind gene regulation must be first introduced. The typical steps of gene regulation includes polymerization, promoter binding, transcription, and translation [14,15]. In the polymerization process, n molecules of transcription factor T combine together to form a active transcription factor T_n for promoter binding, which is described by the chemical reaction as [16]

$$nT \rightleftarrows T_n. \tag{1}$$

In the promoter binding process, the active transcription factor T_n binds to the promoter P on DNA to activate the promoter via the chemical reaction as

$$T_n + P \rightleftarrows C, \tag{2}$$

which leads RNA polymerase attaching to the promoter.

In the transcription process, the information that determines the protein type, is coded on the DNA, and will be copied to mRNA via

$$P + RNAP \rightarrow P + RNAP + mRNA, \tag{3}$$

or

$$C + RNAP \rightarrow C + RNAP + mRNA, \tag{4}$$

where P is the inactivated promoter, and C is the activated promoter. If the transcription factor is an activator, it results in a boost in mRNA production rate; if the transcription factor is a repressor, then the mRNA production rate degrades.

The information on mRNA determines the number, the order, and the type of the aminoacids, which are the basic components constituting protein [17]. The ribosomes bind to the mRNA to initiate the translation process, and mRNA is translated to output protein via

$$mRNA + rRNA \rightarrow mRNA + rRNA + Y, \tag{5}$$

where Y is also called the gene product.

2) Gene Regulation Network: From the perspective of the whole gene regulation process, the activator improves the transcription rate of gene, whereas the repressor degrades the transcription rate of gene. In fact, the transcription factor proteins are themselves encoded by genes, which are regulated by other transcription factors, which in turn may be regulated by other transcription factor. This forms a gene regulation network, which describes all the regulatory transcription interactions in a cell [11].

This network represents a dynamic system, where the input signal triggers the change in the transcription factor activities, and then lead to the changes in the transcription factor. The most simple component in gene regulation network is the single transcription interaction. As in Fig. 17 and Fig. 18, the input signal S_x accelerates the conversion from X to X^*. In Fig. 17, X is the activator, as X^* binds to the promoter of gene Y, the transcription rate of gene Y increases, and the produced protein Y increases. This transcription interaction in the network is described by

$$X \rightarrow Y. \tag{6}$$

In Fig. 18, X is the repressor, as X^* binds to the promoter of gene Y, the transcription rate of gene Y decreases, and the produced protein Y decreases. This transcription interaction in the network is described by

$$X \dashv Y. \tag{7}$$

3) Feed-Forward Loop Network: The above subsections focus on a single transcription interaction, however, live transcription network is composed of many transcription interactions. Network motifs define a way to detect building-block patterns in complex network, and are the patterns that occur more frequently in real network than randomized networks [8]. The FFL is a strong network motif among all three-node patterns, which occurs much often than at random [8,9].

In the structure of FFL, the transcription factor X regulates the other two transcription factors Y and Z, and the transcription factor Y also regulates Z. Depends on the function of regulation, either activation or repression, there are 8 different types of FFLs [10]. Among them, the incoherent type I FFL (I1-FFL) can act as a pulse generator [9].

As shown in Fig. 19, the input signal S_x accelerates the conversion from X to X^*. On one hand, the active transcription factor X^* binds the Z promoter, can initiates the transcription, and increases the production of protein Z. On the other hand, the active transcription factor X^* binds its DNA site in the Y promoter in seconds. With the presence of S_y, the protein Y transits to its active form Y^*. As the repressor Y^* accumulates over time, and surpasses its repression threshold for Z, it binds to the Z promoter, and degrades the production rate of protein

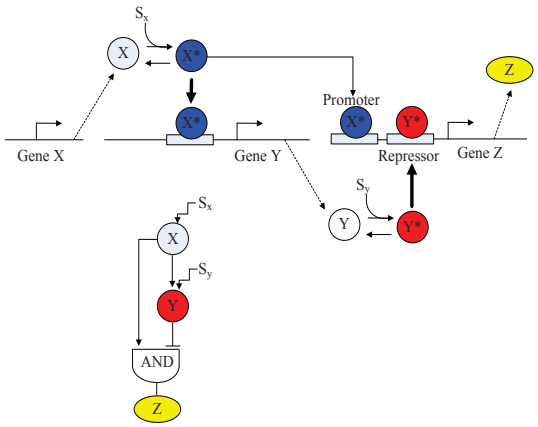

Fig. 5. I1-FFL.

Z. In such a way, X initializes the rapid production of Z first, and after a delay, enough Y accumulates and represses the production of protein Z, which generates a pulse shape for the concentration of protein Z versus time.

One example of I1-FFL is the galactose system of $E.coli$, where the galactose utilization operon $galETK$ is regulated in an I1-FFL by the promoter CRP (X), and the repressor $GalS$ (Y) [12]. Their results shown that a pulse-like response of galETK promotor initiated by the step function input of $cAMP$ (S_x) can be measured via green fluorescent protein (GFP).

One major problem with the transcription regulation is its slow response time, which is usually in the order of cell generation time for the proteins that are not degraded as indicated in [12, Fig. 4]. Several ways to speed up the response time has been proposed, such as using negative autoregulation or incoherent FFL, however, the improved level of response time (hour) is still considered to be slow for realizing efficient molecular communication system due to the inherent drawback of gene regulation [10].

C. FFL-inspired Chemical Circuits

Inspired by the I1-FFL mechanism in gene regulation network, we explore the potential realization of I1-FFL via chemical reactions, in order to achieve fast response time for molecular communication system. A stochastic chemical reaction network is defined as a finite set of reactions involving a finite number of species [18], where these reactions occur in a well-stirred environment, aiming to compute any function or algorithm via molecular progamming. Specific chemical reaction networks have already been designed for signal restoration, noise cleanser, and finite automata, respectively [19].

The three transcription interactions in gene regulation network in I1-FFL can be expressed as

$$X \overset{S_x}{\mapsto} X^*, \tag{8}$$

$$Y \overset{S_y}{\mapsto} Y^*, \tag{9}$$

$$\text{and } X^* + Y^* \mapsto Z, \tag{10}$$

where X^* and Y^* are activated promoters, and Z is the output signal.

To execute I1-FFL with chemical reactions as that in gene regulation network, we define three chemical reactions that corresponding to the above three transcription interactions in gene regulation network as

$$\text{Reaction I} : X + S_y \rightarrow Y, \tag{11}$$

$$\text{Reaction II} : X + S_p \rightarrow P, \tag{12}$$

$$\text{and Reaction III} : Y + P \rightarrow Z, \tag{13}$$

where X, S_p, P, S_y, Y, and Z are distinct chemical species that only allow the above three reactions happen, and P is the output signal.

The chemical reactions in (11) and (12) achieve the similar function as that of the gene regulation in (8) and (9), which are producing new types of protein. In the I1-FFL gene regulation network, the activator X^* in (10) first boosts the generation of protein Z, and only when the repressor Y^* accumulating and surpassing a threshold will leads to the degradation of protein Z, which form a pulse-shape of output signal Z. Different from (10), the chemical reactions in (11), (12), and (13) happen almost simultaneously, which makes the first-increase-then-decrease trend of output signal P unnoticed. To generate a pulse of P, a delay in the arrival of Y is needed, which is enabled by delaying the Reaction II in (12). Motivated by this, we propose a microfluidic device, which can control input signal, chemical reaction, and delayed flow arrival, to realize the same functionality of I1-FFL as gene regulation network (pulse generator) in Fig. 6.

D. Novel Microfluidic Design

In this subsection, we describe each component of our proposed microfluidic device. As we already mentioned in the designed chemical circuits, we will have six types of species: input triggering signal X, continuous supply species S_p and S_y, intermediate species Z and P, and the output signal Y.

1) Y Junction: The reactions between reactants require mixing to occur in a short distance, which can be facilitated by diffusion in Y junctions. Y junctions are configured by one outlet and two inlets as shown in Y junction I and Y-junction II in Fig. 6, where the angle between the main channel and the first inlet starting anticlockwise from the main channel is 45^o. Fluid flow are infused at each branch of the Y-junction by means of a syringe pump, which usually can be described by a square pulse signal with the width depending on the length of injection time.

The fluid flow containing input reactant X with concentration C_{X_0} is injected into the inlet II and inlet III with velocity

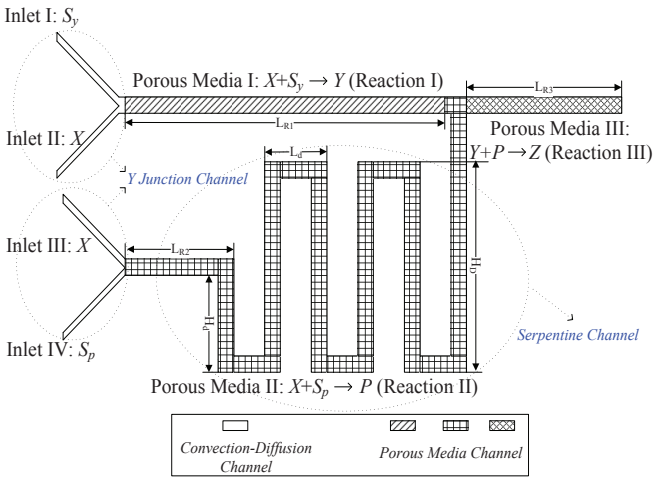

Fig. 6. Novel Microfluidic Device for Pulse Generation.

v using syringe pumps during the ON input signal period T_{ON}, whereas reactant S_y with concentration C_{y_0} and reactant S_p with concentration C_{p_0} are inserted into the inlet I and inlet IV all the time, respectively. By doing so, the flows from inlet I and inlet IV can flush the microfluidic device continuously without influencing Reaction III in (13).

2) Reacting Flow in Porous Media: A porous medium is characterized by a partitioning of the total volume into solid (e.g. a sponge or bundles of capillaries) matrix and pore space, where the pore space is filled by the flow. The mechanic processes responsible for mixing the reactants in porous media considered are advection and diffusion, which facilitates the occurrence of chemical reactions.

The outflow of Y-junction I passes through the porous media channel I with length L_{R1} to realize the Reaction I in (11) to generate the output signal Y, and the outflow of Y-junction II passes through the porous media channel II with length L_{R2} to realize the Reaction II (12) to generate P. Once P arrives at the porous media channel III with length L_{R3}, Reaction III (13) occurs to decrease the output signal Y.

3) Convection-Diffusion Channel: Except from these three porous media channels, four inlet channels are convection-diffusion channels for continuous flow.

4) Serpentine Channel: After the flow propagating through the porous media channel II, the serpentine channel is designed to delay the arrival of P in compact space of microfluidic device, and thus delays the output signal degradation in Chemical Reaction III. The maximum length of serpentine channel is denoted as L_d, and the maximum and the minimum height of serpentine channel is denoted as H_D and H_d, respectively. We name Fig. 6 as the design with 2 delay lines, due to its two complete sine pulses in the serpentine channel.

III. Theoretical Model for Microfluidic Channel

In this section, we first describe the basic characteristics of microfluidic channel, and then provide the analytical model for each main component of proposed microfluidic device to reveal theoretical insights.

A. Basic Characteristics of Microfluidic Channel

The scaling law is introduced to reveal the physical properties of microsystems, which expresses the variation of physical quantities with size l of the microsystems with time, pressure as constant. The scaling law of two classes of forces is expressed as [20]

$$\frac{\text{surface forces}}{\text{volume forces}} \propto \frac{l^2}{l^3} \to \infty, (l \to 0). \tag{14}$$

This scaling law reveals that the volume forces become negligible compared with surface forces, when scaling down to microscale in Microfluidic device.

In physics, the motion of viscous fluid flow inside microfluidic channels is described by the Navier-Stokes equation as [21]

$$\rho\left(\frac{\partial \mathbf{u}}{\partial t}\right) + \rho\left(\mathbf{u}\cdot\nabla\right)\mathbf{u} = -\nabla p + \mu\nabla^2\mathbf{u} + \mathbf{F}, \tag{15}$$

where ∇ is Nabla vector differential operator, $\mathbf{u}$ is the fluid velocity field, ρ is the density of the liquid in the order of 10^3 $\mathrm{kg/m^3}$, p is the pressure, $\mathbf{F}$ is the external force per unit mass, and μ is the constant viscosity of the liquid. This equation relates the velocity to the pressure.

Usually, the Navier-stoke equations are very complicated to solve in closed form. Luckily, they can be simplified, and its analytical solutions can be obtained in some special cases, such as incompressible fluid ($\nabla\cdot\mathbf{u} = 0$), steady flow (all changes of fluid properties with time are zero), and laminar flow ($(\mathbf{u}\cdot\nabla)\mathbf{u} = 0$). The flow where the turbulence is not exhibited is called laminar flow, in this case, the fluid velocity field and the velocity field gradient are orthogonal, and the flow is unidirectional throughout an infinite channel [22].

The nature of the flow highly depends on the Reynolds number, which is the most famous dimensionless parameter in fluid mechanics. For flow in a pipe, the Reynolds number is defined as [20]

$$\mathrm{Re} = \frac{\rho u D_H}{\mu}, \tag{16}$$

where D_H is the hydraulic diameter of the pipe, and u is the area-averaged velocity of the fluid ($\mathrm{m/s}$).

The Reynolds number captures the ratio of the inertia force on an element of fluid to the viscous force on an element. For large Reynolds number, the viscous forces are small relative to inertia forces. For very small Reynolds number ($\mathrm{Re} \ll 1$), the viscous forces are dominant compared with the inertia force. In microfluidic channel, the hydraulic diameter of the pipe and the area-averaged velocity of the fluid are relatively small, as such, the fluid flows are mostly at very low Reynolds number ($\mathrm{Re} < 1$), and the inertia force, such as gravity and turbulence, are negligible [23,24].

B. Analytical Approximation for Microfluidic Component

In microfluidic channel, it is noted that when the distance l from the inlet of channel and the pipe radius r follows $l/r \gg \mathrm{Re}$, the laminar flow can be treated with unidirectional flow, and the infinite channel analysis can be used for the analysis of finite length channel [20,25].

To capture the dispersion of a moving fluid in the microfluidic channel, we first present the analytical model of the convection-diffusion channel with unidirectional flow and constant average velocity throughout the length of flow field.

1) Convection-Diffusion Channel: For a semi-infinite medium with source point $x = 0$, the convection-diffusion channel is characterized by [26]

$$D\frac{\partial^2 C(x,t)}{\partial x^2} - v\frac{\partial C(x,t)}{\partial x} = \frac{\partial C(x,t)}{\partial t}, \tag{17}$$

where D is the diffusion coefficient, v is the average velocity of fluid, and $C(x,t)$ is the molecular concentration in the fluid.

The molecules are injected continuously at the source of channel $x = 0$, thus the first initial boundary condition is

$$C(0,t) = C_0; t \geq 0. \tag{18}$$

At $t = 0$, the molecular concentration in any positions is zero, thus the second initial boundary condition is

$$C(x,0) = 0; x \geq 0. \tag{19}$$

The concentration at locations far away from the source equals zero, thus the third boundary condition is

$$C(\infty,t) = 0; t \geq 0. \tag{20}$$

To simplify the convection-diffusion equation, we perform the transformation on (17) using

$$C\left(x,t\right) = \Upsilon\left(x,t\right)\exp\left(\frac{vx}{2D} - \frac{v^2 t}{4D}\right) \tag{21}$$

to obtain the problem I as

$$\frac{\partial \Upsilon\left(x,t\right)}{\partial t} = D\frac{\partial^2 \Upsilon\left(x,t\right)}{\partial x^2} \tag{22}$$

with the boundary conditions as

$$\Upsilon(0,t) = C_0\exp\left(\frac{u^2 t}{4D}\right); t \geq 0, \tag{23}$$

$$\Upsilon(x,0) = 0; x \geq 0, \tag{24}$$

$$\Upsilon(\infty,t) = 0; t \geq 0. \tag{25}$$

We can see that (22) is in the form as Fick's second law, and thus can be solved analytically.

To solve problem I, we set the first boundary condition as

$$\Upsilon_u(0,t) = 1; t \geq 0, \Rightarrow \Upsilon_u\left(0,t\right) = u\left(t\right), \tag{26}$$

with other two boundary conditions unchanged, where $u\left(t\right)$ is the step function.

To solve the solution $\Upsilon(x,t)$, we perform the Laplace transform on (22) using

$$\widetilde{\Upsilon}\left(x,s\right) = \int_0^\infty e^{-st}\Upsilon\left(x,t\right)dt, \tag{27}$$

and obtain

$$s\widetilde{\Upsilon}\left(x,s\right) = D\frac{\partial^2 \widetilde{\Upsilon}\left(x,s\right)}{\partial x^2}. \tag{28}$$

According to (28) and the second boundary condition in (24), we derive

$$\widetilde{\Upsilon}\left(x,s\right) = g\left(x\right)\exp\left(-\sqrt{\frac{s}{D}}x\right), \tag{29}$$

where $g\left(x\right)$ needs to satisfy the first boundary condition in (26).

The Laplace transform performed on (26) yields

$$\widetilde{\Upsilon}_u\left(0,s\right) = \frac{1}{s}. \tag{30}$$

Combining (29) and (30), we obtain

$$\widetilde{\Upsilon}_u\left(x,s\right) = \frac{1}{s}\exp\left(-\sqrt{\frac{s}{D}}x\right). \tag{31}$$

Applying the inverse Laplace transform leads to the solution as

$$\Upsilon_u\left(x,t\right) = 1 - \text{erf}\left(\frac{x}{2\sqrt{Dt}}\right). \tag{32}$$

Remind that the solution in (32) is solved under the unit initial concentration. To obtain the solution for the problem I with time dependent surface condition at the source, we apply the Duhamel's theorem as

$$\Upsilon\left(x,t\right) = \int_0^t h\left(\tau\right)\frac{\partial}{\partial t}\Upsilon_u\left(x,t-\tau\right)d\tau, \tag{33}$$

where $h\left(t\right)$ is the initial surface concentration with

$$h(t) = C_0\exp\left(\frac{v^2 t}{4D}\right). \tag{34}$$

Substituting (32) and (34) into (33), we derive

$$\begin{aligned}\Upsilon\left(x,t\right) =& C_0\frac{2}{\sqrt{\pi}}e^{\frac{v^2 t}{4D}}\left[\int_0^\infty \exp\left(-\tau^2 - \left(\frac{vx}{4D\tau}\right)^2\right)d\tau\right.\\ &\left. - \int_0^{\frac{x}{2\sqrt{Dt}}}\exp\left(-\tau^2 - \left(\frac{vx}{4D\tau}\right)^2\right)d\tau\right].\end{aligned} \tag{35}$$

After some mathematical manipulations, we obtain the solution of the problem I as

$$\begin{aligned}\Upsilon\left(x,t\right) =& \frac{C_0}{2}e^{\frac{v^2 t}{4D}}\left[e^{\frac{vx}{2D}}\text{erfc}\left(\frac{x}{2\sqrt{Dt}} + \frac{v\sqrt{t}}{2\sqrt{D}}\right)\right.\\ &\left. + e^{-\frac{vx}{2D}}\text{erfc}\left(\frac{x}{2\sqrt{Dt}} - \frac{v\sqrt{t}}{2\sqrt{D}}\right)\right].\end{aligned} \tag{36}$$

Substituting (36) into (21), we derive

$$C\left(x,t\right) = \frac{C_0}{2}\left[\text{erfc}\left(\frac{x-vt}{2\sqrt{Dt}}\right) + e^{\frac{vx}{D}}\text{erfc}\left(\frac{x+vt}{2\sqrt{Dt}}\right)\right]. \tag{37}$$

To verify the accuracy of the derived analytical concentration in (37), in Fig. 7, we plot the analytical concentration at distance $x = 0.005\mu$m away from the source at $x = 0$ with $C_0 = 1.5$ mol/m^3 using (37). The simulation points in Fig. 7 are plotted using the outlet molecular concentration of a square microfluidic tube with the depth and the height as $d = h = 10^{-5}$m, and the width as $w = 0.005$m in COMSOL simulation, where the molecular concentration $C_0 = 1.5$ mol/m^3 are injected at the inlet of the microfluidic tube with velocity $v = 0.002$m/s. As can be seen from Fig. 7, the analytical curve matched well with the COMSOL simulation, which showcases the correctness of the analytical solution in (37). As expected, the outlet molecular concentration increases with increasing time, and reaches the saturated concentration C_0.

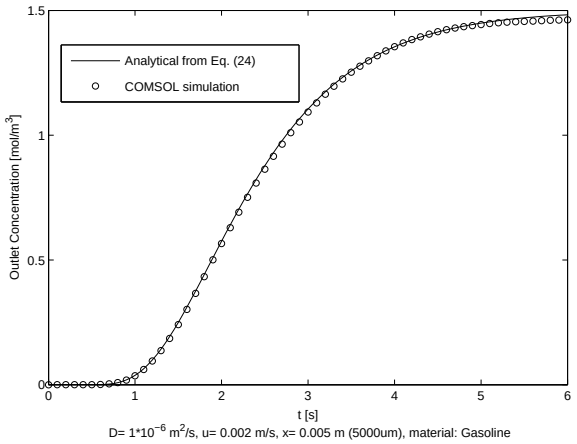

Fig. 7. Outlet concentration of the convection-diffusion channel versus time.

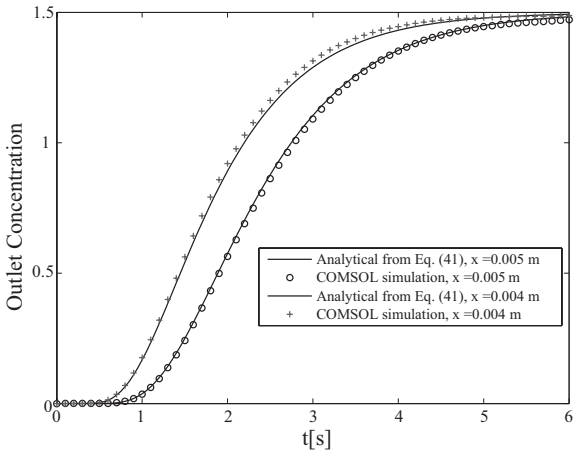

Fig. 8. Outlet concentration of P in the convection-diffusion-reaction channel versus time.

2) Convection-diffusion-reaction Channel: To quantitatively describe the chemical reaction and dispersion of chemical species in porous media of microfluidic device, we introduce one-dimensional convection-diffusion-reaction equation. For the second-order reactions occur in the porous media, the species S_p and S_y are continuously supplied and abundant, thus we can assume there is no significant change in the concentration of the species S_p and S_y throughout the process, and the concentration of species S_p and S_y can be approximated as time invariant constant.

For the microfludic porous media device with low Reynolds number (Re$\ll$1), its convective-dispersive equation with chemical reaction $X + S_y \rightarrow Y$ is described as

$$D\frac{\partial^2 C_X(x,t)}{\partial x^2} - v\frac{\partial C_X(x,t)}{\partial x} = \frac{\partial C_X(x,t)}{\partial t} - k_1 C_X(x,t) C_{S_y}, \tag{38}$$

$$D\frac{\partial^2 C_Y(x,t)}{\partial x^2} - v\frac{\partial C_Y(x,t)}{\partial x} = \frac{\partial C_Y(x,t)}{\partial t} + k_1 C_X(x,t) C_{S_y}, \tag{39}$$

where k_1 is the reaction rate.

The species X is injected at the inlet of microfludic device $x = 0$, thus the first initial boundary condition is

$$C_X(0,t) = C_{X_0}; t \geq 0 \Rightarrow C_X(0,t) = C_{X_0} u(t). \tag{40}$$

At $t = 0$, the concentration of species X in any positions is zero, thus the second initial boundary condition is

$$C_X(x,0) = 0; x \geq 0. \tag{41}$$

The concentration change over locations far away from the source equals zero, thus the third boundary condition is

$$\frac{\partial C_X(\infty,t)}{\partial x} = 0; t \geq 0. \tag{42}$$

The solution can be obtained by first taking the Laplace transform of Eqs. (38), (40), and (41) using

$$\widetilde{C}_X(x,s) = \int_0^\infty e^{-st} C_X(x,t)\, dt. \tag{43}$$

The Laplace transform of (38) satisfying (41) is

$$D\frac{\partial^2 \widetilde{C_X}(x,s)}{\partial x^2} - v\frac{\partial \widetilde{C_X}(x,s)}{\partial x} = \left(s + k_1 C_{S_y}\right) \widetilde{C_X}(x,s). \tag{44}$$

The Laplace transform of (40) and (42) are

$$\widetilde{C_X}(0,s) = \frac{C_0}{s}, \tag{45}$$

and

$$\frac{\partial \widetilde{C_X}(\infty,s)}{\partial x} = 0. \tag{46}$$

Combining (43), (44), and (46), we derive

$$\widetilde{C_X}(x,s) = \frac{C_0}{s} \exp\left[\frac{vx}{2D} - x\sqrt{\frac{v^2}{4D^2} + \frac{s + k_1 C_{S_y}}{D}}\right]. \tag{47}$$

Taking the inverse Laplace transform of (47), we derive

$$C_X(x,t) = \frac{C_0}{2}\left\{\exp\left[\frac{(v-\alpha)\,x}{2D}\right]\operatorname{erfc}\left[\frac{x-\alpha t}{2\sqrt{Dt}}\right] + \exp\left[\frac{(v+\alpha)\,x}{2D}\right]\operatorname{erfc}\left[\frac{x+\alpha t}{2\sqrt{Dt}}\right]\right\}, \tag{48}$$

where $\alpha = \sqrt{v^2 + 4k_1 C_{S_y} D}$.

To derive the concentration of species Y, we combine (38) and (39) as

$$D\frac{\partial^2 C_s(x,t)}{\partial x^2} - v\frac{\partial C_s(x,t)}{\partial x} = \frac{\partial C_s(x,t)}{\partial t}, \tag{49}$$

where $C_s(x,t) = C_X(x,t) + C_Y(x,t)$. Interestingly, this equation becomes the convection-diffusion equation.

The sum concentration of X and Y follows the three boundary conditions

$$C_s(0,t) = C_0; t \geq 0, \tag{50}$$

$$C_s(x,0) = 0; x \geq 0, \tag{51}$$

$$C_s(\infty,t) = 0; t \geq 0. \tag{52}$$

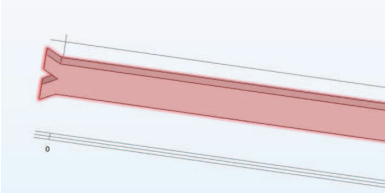

Fig. 9. Y junction design.

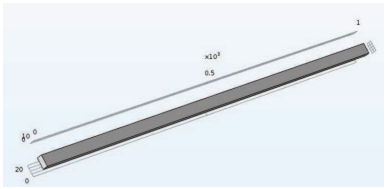

Fig. 10. Equivalent Y junction design.

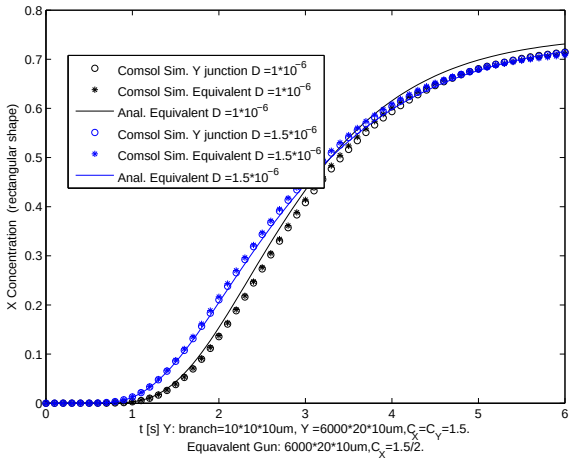

Fig. 11. Outlet concentration of X (S_p) in the Y junction channel versus time.

Following the same derivations in Section III. B. 1, we have the solution for (49) under the above boundary conditions as

$$C_s\left(x,t\right)=\frac{C_0}{2}\left[\operatorname{erfc}\left(\frac{x-vt}{2\sqrt{Dt}}\right)+e^{\frac{vx}{D}}\operatorname{erfc}\left(\frac{x+vt}{2\sqrt{Dt}}\right)\right]. \tag{53}$$

Taking the deduction of $C_X(x,t)$ in (48) from $C_s\left(x,t\right)$ in (53), we derive the concentration of Y as

$$\begin{aligned}C_Y\left(x,t\right)=&\frac{C_0}{2}\left\{\operatorname{erfc}\left(\frac{x-vt}{2\sqrt{Dt}}\right)+e^{\frac{vx}{D}}\operatorname{erfc}\left(\frac{x+vt}{2\sqrt{Dt}}\right)\right.\\&-\exp\left[\frac{\left(v-\alpha\right)x}{2D}\right]\operatorname{erfc}\left[\frac{x-\alpha t}{2\sqrt{Dt}}\right]\\&\left.-\exp\left[\frac{\left(v+\alpha\right)x}{2D}\right]\operatorname{erfc}\left[\frac{x+\alpha t}{2\sqrt{Dt}}\right]\right\},\end{aligned} \tag{54}$$

where $\alpha=\sqrt{v^2+4k_1C_{S_y}D}$.

In Fig. 8, we plot the analytical concentration of species P in (54) with parameters $x=0.005\mu$m, $C_{X_0}=1.5$ mol/m^3, $k_1=1000$m/s, and $D_X=D_{S_y}=D_Y=1\times10^{-6}$m^2/s. The simulation points in Fig. 8 are plotted using the outlet molecular concentration of species Y in a porous media with reaction $X+S_y\rightarrow Y$ happens throughout the square microfluidic tube with $d=h=10^{-5}$m in COMSOL simulation, where the molecular concentration of X ($C_{X_0}=1.5$ mol/m^3) is injected at the inlet of the microfluidic tube with velocity $v=0.002$m/s. As can be seen, the simulation points are in precise agreement with the analytical curves. The outlet concentration of Y increases and reaches the maximum due to the high reaction rate k_1. Furthermore, the longer the microfluidic tube, the slower the outlet concentration of Y increases, and the lower concentration of of Y.

3) Y Junction Channel: In our design, the Y junction channel is an important interconnection configuration for combining two channels. In Fig. 9, we plot the Y junction channel with square tube in COMSOL, where the depth, the height, and the width of each subchannel are $d_i=h_i=w_i=10^{-5}$m, and that of the combined channel are $d_c=10^{-5}$m, $h_c=2\times10^{-5}$m, and $w_c=0.006$m.

The species X and the species S_p are injected into two inlets of Y junction channel $x=0$ with the same velocity v, thus the first initial boundary conditions are

$$C_X(0,t)=C_{X_0};t\geq0\Rightarrow C_X(0,t)=C_{X_0}u\left(t\right), \tag{55}$$

and

$$C_{S_p}(0,t)=C_{S_{p0}};t\geq0\Rightarrow C_{S_p}(0,t)=C_{S_{p_0}}u\left(t\right), \tag{56}$$

where $C_{X_0}=C_{S_{p0}}$.

As the length of the subchannel is much smaller than that of combined channel, and no reaction happens in the Y junction channel, injecting the same volume and concentration of independent species X or S_p into two subchannels can be treated as diluting species X using S_p, or diluting species S_p using X. Thus, the outlet concentration of X or S_p in Fig. 9 can be approximately equivalent to that of a straight channel in Fig. 10 with half of inlet concentration, and geometry $d_c=10^{-5}$m, $h_c=2\times10^{-5}$m, and $w_c=0.006$m. Therefore, the outlet concentrations of species X and S_p in the Y junction channel in Fig. 9 can be approximated as

$$\begin{aligned}C_X\left(x,t\right)=&C_{S_p}\left(x,t\right)=\\&\frac{C_e}{2}\left[\operatorname{erfc}\left(\frac{x-vt}{2\sqrt{Dt}}\right)+e^{\frac{vx}{D}}\operatorname{erfc}\left(\frac{x+vt}{2\sqrt{Dt}}\right)\right],\end{aligned} \tag{57}$$

where $C_e=\frac{C_{X_0}}{2}$.

In Fig. 11, we plot the analytical curves using (57), the simulation points using the COMSOL designs in Fig. 9 and Fig. 10, with velocity $v=0.002$m/s and diffusion coefficient $D_X=D_{S_p}=D$. The inlets of Y junction channel in Fig. 9 are injected with the concentration of X and S_p as $C_{X_0}=C_{S_{p_0}}=1.5$mol/m^3. The inlet of equivalent Y junction channel in Fig. 10 is injected with the concentration of X as $\frac{C_{X_0}}{2}$. It is shown that the COMSOL simulation and analytical results for the outlet concentration of equivalent Y junction design can well approximate the COMSOL simulation for the outlet concentration of Y junction design. We also see that the outlet concentration first increases and then decreases with increasing the diffusion coefficient as the time goes on.

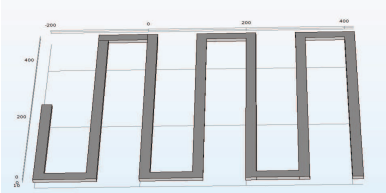

Fig. 12. Serpentine channel.

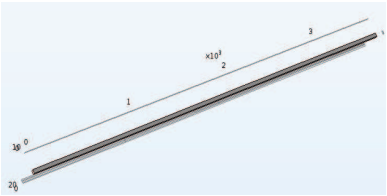

Fig. 13. Equivalent serpentine channel.

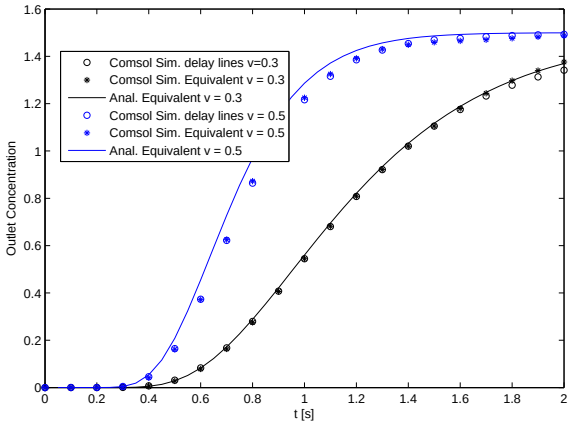

Fig. 14. Outlet concentration in the serpentine channel versus time.

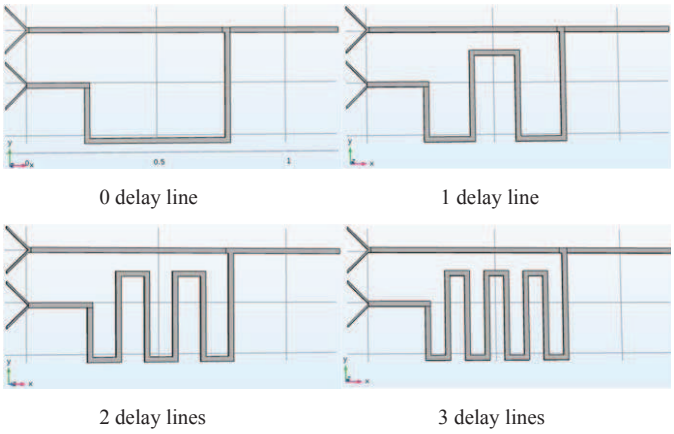

Fig. 15. Four delay lines.

4) Serpentine Channel: In our design, the serpentine channel are used to delay the arrival time of species P, and the number of delay lines determine the length of delay in arrival time of P [27,28]. The turning channel in the delay lines usually causes different laminas propagating with different lengths, however, when the channel is in low Reynolds number with very small side length tube, we can approximate the outlet concentration of the delay lines channel as that of straight channel with equivalent length. Fig. 12 is the serpentine channel having 3 delay lines with $L_d = 0.12 \times 10^{-3}$m, $H_D = 0.25 \times 10^{-3}$m, $H_d = 0.5 \times 10^{-3}$m, $d_d = 10^{-5}$m, and $h_d = 2\times10^{-5}$m. Fig. 13 is the equivalent straight channel with $d_d = 10^{-5}$m, $h_d = 2\times10^{-5}$m, and width $w_d = 3.73\times10^{-3}$m, where w_d is calculated by taking the sum of the length in delay lines channel.

In Fig. 14, we plot the outlet concentration of the delay lines design in Fig. 12 and that of the equivalent delay lines design in Fig. 13 using COMSOL. In the COMSOL simulation of both designs, the initial concentration $C_{X_0} = 1.5$ mol/m^3 is injected with velocity v in the left inlet, and the outlet concentrations are recorded. We find that the simulation points well matched with each other, and reveal that the outlet concentration of equivalent delay lines can well approximate that of delay lines. As expected, increasing the velocity largely improves the outlet concentration.

IV. Numerical Results

In this section, we provide a numerical evaluation of the proposed microfluidic device for pulse generation.

A. COMSOL Multiphysics Implementation

To examine the pulse generation characteristics of our microfluidic device design in Fig. 6, we implement this design in COMSOL according to the geometry in Fig. 15 with different number of delay lines in four subfigures. In Fig. 15, these four subfigures are with the same geometry parameters as in Table I except the serpentine channel in Table II. The reacting flow in porous media module in COMSOL is applied to realize the chemical reactions I, II, and III. Unless specified, we assume

TABLE I
The Parameters of Proposed Microfludic Design.

Channel	Length (μm)	Width (μm)	Depth (μm)
Inlet Y junction	$80\sqrt{2}$	10	10
Outlet Y junction Porous media I	1200	20	10
Outlet Y junction Porous media II	240	20	10
Porous media I channel	740	20	10
Porous media III channel	420	20	10

diffusion coefficient for each species as $D = 10^{-6}$m^2/s, the velocity for each inlet channel as $v = 0.002$m/s, the reaction rate for each reaction as $k_1 = 0.66971$m/s, and the initial concentration as $C_{X_0} = 4$mol/m^3, $C_{S_{P0}} = 4$mol/m^3, and $C_{S_{y_0}} = 3$mol/m^3.

B. Pulse Shaping

In Fig. 16, we plot the inlet concentration of X and the outlet concentration of Y versus time for four microfludic designs in Fig. 15. The input signal is a square pulse-like signal generated by syringe pump with concentration C_{X_0} normalized to one and duration as 2s. It is interesting to see that the output pulses can be generated successfully during the ON input signal, and the tail of pulse decays to zero

TABLE II
THE PARAMETERS OF SERPENTINE CHANNEL IN FIG. 15.

Channel	L_d (μm)	H_D (μm)	H_d (μm)
0 delay line	560	0	210
1 delay line	220	350	210
2 delay lines	128	350	210
3 delay lines	97	350	210

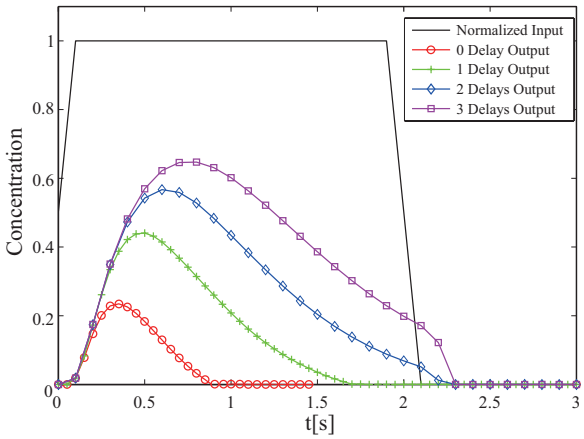

Fig. 16. Concentration of input and output signals in FFL-inspired microfluidic device versus time.

during the OFF input period, in less than 0.2s. We also notice that increasing the number of delay lines increases the maximum concentration of output signal Y, which is due to the later arrival of P at Porous media channel III, resulting from the increasing length of serpentine channel, gives more time for Reaction I to generate Y. It is seen that the longer the serpentine channel, the wider the generated pulse, due to that longer time is given to generate Y in Reaction I, and more Y needs to be consumed in Reaction III. This is also indicated by the observation in Fig. 8, where the longer the serpentine channel results in the lower concentration of P, and thus longer time to degrade the generated Y.

These observations showcase that the number of delay lines in serpentine channel can be well-designed to shape the pulse. The narrow pulses generated by 0&1 delay lines in serpentine channel may reduce the intersymbol interference during the receiver detection, whereas the wide pulses generated by 2&3 delay lines in serpentine channel result in stronger received signal with more precise pulse coverage in terms of time.

In Fig. 17, we plot the outlet concentration of Y for the microfludic design with 2 delays lines as in Fig. 15 versus time for various diffusion coefficient D. The input signal is a step function pulse starts at $t = 0$. We see that increasing the diffusion coefficient does not change the maximum concentration of Y aggressively, but increases the steady-state outlet concentration of output signal largely. This can be contributed to the fact that the higher diffusion coefficient results in large displacement, and the generated Y in Reaction I leaves the device much faster before they are totally consumed by Reaction III. Besides, the outlet concentration of output signal stables approximately similar time for various diffusion coefficient. From the perspective of molecular communication

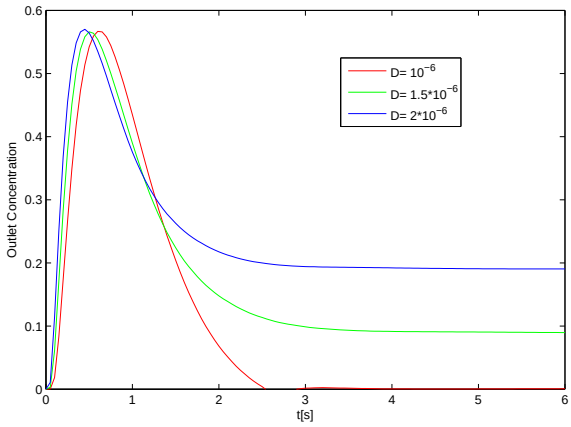

Fig. 17. Concentration of output signals in FFL-inspired microfluidic device versus time.

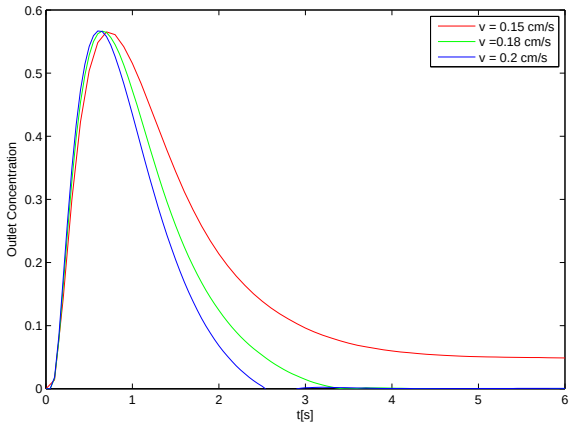

Fig. 18. Concentration of output signals in FFL-inspired microfluidic device versus velocity.

design, the higher tail of Y due to higher diffusion coefficient will introduce larger intersymbol interference, and harms the reliable transmission.

In Fig. 18, we plot the outlet concentration of Y for the microfludic design with 2 delays lines as in Fig. 15 versus time for various fluid velocities v. The input signal is a step function pulse starts at $t = 0$. We observe that the slower the velocity of fluid, the outlet concentration of output signal stables at higher concentration, rather than zero concentration, which is mostly due to the late arrival of P to consume Y in Reaction III. It is thus revealed that the velocity needs to be well-tuned to generate the pulse right inside ON input signal duration.

In Fig. 19, we plot the outlet concentration of Y for the microfludic design with 2 delays lines as in Fig. 15 versus time for various initial concentration of S_p. The input signal is a square-pulse with duration 2s. We observe that increasing the initial concentration of S_p increases the degradation speed of the concentration of Y, due to the increased concentration of P generated to react with Y in Reaction III. We also see that the maximum outlet concentration of output signal increases

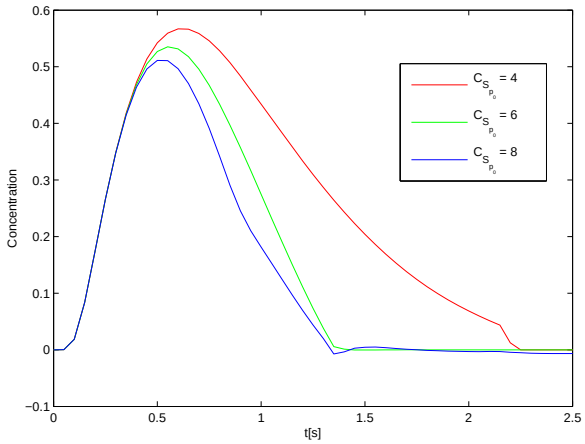

Fig. 19. Concentration of output signals in FFL-inspired microfluidic device versus input concentration of S_{p0}.

with decreasing the initial concentration of S_p, which can be contributed to the degraded concentration of P participating in Reaction III for output signal degradation. The observation that the higher concentration and wider pulse of the output signal generated by smaller concentration of Y reveals the energy efficiency of our proposed pulse generator.

V. Conclusion

In this paper, we proposed a pulse generator for MC capable of generating a predefined pulse-shaped molecular concentration upon a triggering input. The design of this pulse generator is motivated by the MC literature on information transmission via molecular pulse modulation, and it is inspired on a motif in cells' gene regulatory networks. The proposed design is based on a microfluidic system with standard and reproducible components, whose design parameters control the shape of the output pulse. Analytical expressions of these components are provided and numerically validated to demonstrate their input-output dependency on standard design parameters, while a simulation-based implementation of the overall design shows how the predefined shaping of the pulse can be controlled at design phase. We envision not only that this pulse generator might be an important components in the design of future MC systems, but also that the methodology presented in this paper will help in the design of additional MC components inspired by biochemical processes and based on microfluidic systems.

Acknowledgment

This work was supported by the US National Science Foundation (NSF) through grant MCB-1449014, and the NSF Nebraska EPSCoR through the First Award grant EPS-1004094.

References

[1] I. F. Akyildiz, F. Brunetti, and C. Blazquez, "Nanonetworks: A new communication paradigm at molecular level," *Computer Networks (Elsevier) Journal*, vol. 52, no. 12, pp. 2260–2279, August 2008.

[2] I. F. Akyildiz, M. Pierobon, S. Balasubramaniam, and Y. Koucheryavy, "The internet of bio-nano things," *IEEE Communications Magazine*, vol. 53, no. 3, pp. 32–40, March 2015.

[3] N. Farsad, H. B. Yilmaz, A. Eckford, C.-B. Chae, and W. Guo, "A comprehensive survey of recent advancements in molecular communication," *IEEE Communications Surveys & Tutorials*, vol. 18, no. 3, pp. 1887–1919, Third Quarter 2016.

[4] Y. Deng, A. Noel, W. Guo, A. Nallanathan, and M. Elkashlan, "Stochastic geometry model for large-scale molecular communication systems," in *Proc. IEEE GLOBECOM*, Dec. 2016.

[5] E. B. Pehlivanoglu, B. D. Unluturk, and O. B. Akan, "Modulation in molecular communications: A look on methodologies," in *Modeling, Methodologies and Tools for Molecular and Nano-scale Communications*. Springer International Publishing, 2017, pp. 79–97.

[6] Y. Deng, A. Noel, W. Guo, A. Nallanathan, and M. Elkashlan, "Analyzing large-scale multiuser molecular communication via 3D stochastic geometry," *IEEE Trans. Mol. Biol. Multi-Scale Commun.*, 2017.

[7] IEEE P1906.1/D2.0, *IEEE Draft Recommended Practice for Nanoscale and Molecular Communication Framework*. IEEE Standards, 2015.

[8] R. Milo, S. Shen-Orr, S. Itzkovitz, N. Kashtan, D. Chklovskii, and U. Alon, "Network motifs: simple building blocks of complex networks," *Science*, vol. 298, no. 5594, pp. 824–827, Oct. 2002.

[9] U. Alon, "Network motifs: theory and experimental approaches," *Nature Reviews Genetics*, vol. 8, no. 6, pp. 450–461, Jun. 2007.

[10] A. Uri, *An introduction to systems biology: design principles of biological circuits*. CRC press, 2006.

[11] G. Karlebach and R. Shamir, "Modelling and analysis of gene regulatory networks," *Nature Reviews Molecular Cell Biology*, vol. 9, no. 10, pp. 770–780, Oct. 2008.

[12] S. Mangan, S. Itzkovitz, A. Zaslaver, and U. Alon, "The incoherent feed-forward loop accelerates the response-time of the gal system of escherichia coli," *Journal of molecular biology*, vol. 356, no. 5, pp. 1073–1081, Mar. 2006.

[13] L. J. Kahl and D. Endy, "A survey of enabling technologies in synthetic biology," *Journal of Biol. Eng.*, vol. 7, no. 1, p. 13, May 2013.

[14] R. Weiss, S. Basu, S. Hooshangi, A. Kalmbach, D. Karig, R. Mehreja, and I. Netravali, "Genetic circuit building blocks for cellular computation, communications, and signal processing," *Nat. Comput.*, vol. 2, no. 1, pp. 47–84, Mar. 2003.

[15] D. Latchman *et al.*, *Gene regulation*. Taylor & Francis, 2007.

[16] B. D. Unluturk, A. O. Bicen, and I. F. Akyildiz, "Genetically engineered bacteria-based biotransceivers for molecular communication," *IEEE Trans. on Commun.*, vol. 63, no. 4, pp. 1271–1281, Apr. 2015.

[17] M. Nei, *Molecular evolutionary genetics*. Columbia university press, 1987.

[18] M. Cook, D. Soloveichik, E. Winfree, and J. Bruck, "Programmability of chemical reaction networks," in *Algorithmic Bioprocesses*. Springer, 2009, pp. 543–584.

[19] T. H. Klinge, "Modular and robust computation with deterministic chemical reaction networks," Ph.D. dissertation, 2016.

[20] H. Bruus, "Theoretical microfluidics. 2008."

[21] R. Temam, *Navier-stokes equations*. North-Holland Amsterdam, 1984, vol. 2.

[22] F. M. White and I. Corfield, *Viscous fluid flow*. McGraw-Hill New York, 2006, vol. 3.

[23] D. Di Carlo, "Inertial microfluidics," *Lab on a Chip*, vol. 9, no. 21, pp. 3038–3046, Sep. 2009.

[24] D. Di Carlo, D. Irimia, R. G. Tompkins, and M. Toner, "Continuous inertial focusing, ordering, and separation of particles in microchannels," *Proc. Natl. Acad. Sci.*, vol. 104, no. 48, pp. 18 892–18 897, Nov. 2007.

[25] B. J. Kirby, *Micro-and nanoscale fluid mechanics: transport in microfluidic devices*. Cambridge University Press, 2010.

[26] T. Stocker, *Introduction to climate modelling*. Springer Science & Business Media, 2011.

[27] X.-D. Wang, X.-X. Zhang, T. Liu, Y.-Y. Duan, W.-M. Yan, and D.-J. Lee, "Channel geometry effect for proton exchange membrane fuel cell with serpentine flow field using a three-dimensional two-phase model," *J. Fuel Cell. Sci. Tech.*, vol. 7, no. 5, p. 051019, Jul. 2010.

[28] J. Feser, A. Prasad, and S. Advani, "On the relative influence of convection in serpentine flow fields of pem fuel cells," *J. Power Sources*, vol. 161, no. 1, pp. 404–412, Oct. 2006.